6834 *Inorg. Chem.* **2010**, *49*, 6834–6839
DOI: 10.1021/ic100445y

Inorganic Chemistry
Article

Hydrothermal Synthesis and Characterization of $LiREF_4$ (RE = Y, Tb−Lu) Nanocrystals and Their Core−Shell Nanostructures

Qiang Zhang and Bing Yan*

Department of Chemistry, Tongji University, 1239 Siping Road, Shanghai 200092, China

Received December 5, 2009

In this paper, a water−ethanol−oleic acid system was developed to prepare $LiREF_4$ nanocrystals with a controlled size and shape. The influence of LiOH concentration and temperature on the phase and shape evolution of the $LiREF_4$ nanocrystals was systematically investigated and discussed. It was found that the LiOH concentration was the key factor responsible for the shape evolution and phase control for $LiREF_4$ nanocrystals at selected temperatures. The $LiYF_4$−$LiLuF_4$ core−shell nanostructure was synthesized and characterized.

Introduction

The complex fluorides $LiREF_4$ (RE = rare earth ion) possess the tetragonal $I4_1/a$ structure of Scheelite $CaWO_4$ with all of the RE ions placed in an identical chemical environment. They are a class of crystal materials with special properties, such as downconversion or upconversion fluorescence,[1,2] the potential for use in lasers,[3] Ising dipolar ferromagnetism,[4,5] and a wide variety of collective quantum effects, ranging from quantum tunneling of single moments and domain walls to quantum annealing, macroscopic quantum entanglement, coherent spin oscillations (Rabi oscillations), quantum phase transition, and the disordered system of a random field.[6−13] Compared with the well-known quantum confinement effect of semiconductor nanocrystals (quantum dots, QDs),[14] the effect of size reduction and shape on the physical behaviors of the dilution series of $LiY_{1-x}Ho_xF_4$ is still in the scale. At the same time, research into magnetic nanostructures with single or finite domain walls is the focus in the identification of domain wall tunneling.[15,16] To pursue such issues, the prerequisite is to synthesize $LiREF_4$ nanostructures with a controlled size and shape in the nanoscale. A unique way to investigate the quantum behaviors of $LiY_{1-x}Ho_xF_4$ stemming from their unique Ising axis and magnetic dipole−dipole interactions among the Ho ions and to increase photoluminescent (PL) efficiency is to synthesize core−shell nanostructures.[17,18] We report here the hydrothermal synthesis and characterization of $LiREF_4$ (RE = Y, Tb−Lu) nanocrystals and their core−shell nanostructures.

$LiYF_4$ nanocrystals less than 100 nm have been synthesized using high-temperature thermal decomposition of lithium trifluoroacetate and yttrium trifluoroacetate.[2,19] Micrometer-sized $LiYF_4$, $LiHoF_4$, and $LiErF_4$ also have been synthesized using the hydrothermal method with noxious hydrogen fluoride.[20,21] However, the limited sizes and simple chemical compositions of these materials may limit their further usage in fundamental and technical fields. Thorough research on the synthesis and characterization of $LiREF_4$ is thus necessary, especially for $LiYF_4$ and $LiHoF_4$. Water−ethanol−oleic

*To whom the correspondence should be addressed. Phone: +86-21-65984663. Fax: +86-21-65982287. E-mail: byan@tongji.edu.cn.

(1) Wegh, R. T.; Donker, H.; Oskam, K. D.; Meijerink, A. *Science* **1999**, *283*, 663.
(2) Mahalingam, V.; Vetrone, F.; Naccache, R.; Speghini, A.; Capobianco, J. A. *Adv. Mater.* **2009**, *21*, 4025.
(3) Santo, A. M. E.; Librantz, A. F. H.; Gomes, L.; Pizani, P. S.; Ranieri, I. M.; Vieira, N. D., Jr.; Baldochi, S. L. *J. Cryst. Growth* **2006**, *292*, 149.
(4) Cooke, A. H.; Jones, D. A.; Silva, J. F. A.; Wells, M. R. *J. Phys. C: Solid State Phys.* **1975**, *8*, 4083.
(5) Ahlers, G.; Kornblit, A.; Guggenhéim, H. J. *Phys. Rev. Lett.* **1975**, *34*, 1227.
(6) Giraud, R.; Wernsdorfer, W.; Tkachuk, A. M.; Mailly, D.; Barbara, B. *Phys. Rev. Lett.* **2001**, *87*, 057203.
(7) Brooke, J.; Bitko, D.; Rosenbaum, T. F.; Aeppli, G. *Science* **1999**, *284*, 779.
(8) Brooke, J.; Rosenbaum, T. F.; Aeppli, G. *Nature* **2001**, *413*, 610.
(9) Ghosh, S.; Parthasarathy, R.; Rosenbaum, T. F.; Aeppli, G. *Science* **2002**, *296*, 2195.
(10) Santoro, G. E.; Martoňák, R.; Tosatti, E.; Car, R. *Science* **2002**, *295*, 2427.
(11) Ghosh, S.; Rosenbaum, T. F.; Aeppli, G.; Coppersmith, S. N. *Nature* **2003**, *425*, 48.
(12) Rønnow, H. M.; Parthasarathy, R.; Jensen, J.; Aeppli, G.; Rosenbaum, T. F; McMorrow, D. F. *Science* **2005**, *308*, 389.
(13) Silevitch, D. M.; Bitko, D.; Brooke, J.; Ghosh, S.; Aeppli, G.; Rosenbaum, T. F. *Nature* **2007**, *448*, 567.
(14) Alivisatos, A. P. *Science* **1996**, *271*, 933.
(15) Thomas, L.; Lionti, F.; Ballou, R.; Gatteschi, D.; Sessoli, R.; Barbara, B. *Nature* **1996**, *383*, 145.
(16) Atkinson, D.; Allwood, D. A.; Xiong, G.; Cooke, M. D.; Faulkner, C. C.; Cowburn, R. P. *Nat. Mater.* **2003**, *2*, 85.
(17) Skumryev, V.; Stoyanov, S.; Zhang, Y.; George, H.; Dominique, G.; Nogués, J. *Nature* **2003**, *423*, 850.
(18) Zhang, Q.; Zhang, Q. M. *Mater. Lett.* **2009**, *63*, 376.
(19) Mai, H. X.; Zhang, Y. W.; Si, R.; Yan, Z. G.; Sun, L. D.; You, L. P.; Yan, C. H. *J. Am. Chem. Soc.* **2006**, *128*, 6426.
(20) Zhao, C. Y.; Feng, S. H.; Xu, R. R.; Shi, C. S.; Ni, J. Z. *Chem. Commun.* **1997**, *10*, 945.
(21) Xun, X.; Feng, S. H.; Xu, R. R. *Mater. Res. Bull.* **1998**, *33*, 369.

Published on Web 06/25/2010

acid/linoleic acid system hydrothermal synthesis has been revealed to have powerful features, to be general for controlled syntheses of many kinds of materials, and to be industrially feasible for its ease and low cost.[22−24] By replacing sodium hydroxide with lithium hydroxide under the above-mentioned water−ethanol−oleic acid system, we can successfully synthesize a series of $LiREF_4$ (RE = Y, Tb−Lu) nanocrystals and their core−shell nanostructures in the temperature range of 110−240 °C.

Experimental Section

Synthesis. The $LiREF_4$ nanocrystals and core−shell nanostructure were hydrothermally prepared by using oleic acid as a stabilizing agent and LiOH, NH_4F, and $RE(NO_3)_3$ as precursors at 110−240 °C. In a typical synthesis of $LiREF_4$, 0.97 g (23 mmol) of $LiOH \cdot H_2O$, 10 mL of H_2O, 18 mL (57 mmol) of oleic acid (90 wt %), and 30 mL of ethanol were mixed well under vigorous stirring at 35 °C. A 4 g solution in deionized water containing 1 mmol of $Y(NO_3)_3$ was added with vigorous stirring until a transparent solution was obtained. Then, 4 mL (4 mmol) of 1 M NH_4F in deionized water was dropped into the above solution, with vigorous stirring maintained for 2 min. Then, the mixture was transferred to a 100 mL Teflon-lined autoclave and heated at 130 °C for 5 h.

The $LiYF_4$−$LiLuF_4$ core−shell nanostructure was synthesized as follows. The core $LiYF_4$ was synthesized according to the above-mentioned method. After the reaction system was cooled naturally to room temperature, 4 g of solution in deionized water containing 1 mmol of $Lu(NO_3)_3$ was added under vigorous stirring; then, 2 mL of 2 M NH_4F in deionized water was dropped in. Then, the autoclave was sealed again and heated to 130 °C for 2.5 h.

The $LiHoF_4$−$LiErF_4$−$LiYF_4$ core−shell nanostructure was synthesized as follows. The core $LiHoF_4$ was synthesized according to the above-mentioned method at 200 °C for 4 h. After the reaction system was cooled naturally to room temperature, 2 g of the solution in deionized water containing 0.5 mmol of $Er(NO_3)_3$ was added under vigorous stirring; then 2 mL of 1 M NH_4F was dropped in. Then, the autoclave was sealed again and heated to 200 °C for 1 h. A 2 g solution in deionized water containing 0.5 mmol of $Y(NO_3)_3$ and 2 mL of 1 M NH_4F was adopted to synthesize the $LiYF_4$ shell at 200 °C for another 1 h.

Iminodiacetic acid and citric acid stabilized nanocrystals were synthesized as follows. A total of 6 mmol of iminodiacetic acid or citric acid and 6 mmol of $LiOH \cdot H_2O$ were dissolved in 20 mL of H_2O. A 4 g solution in deionized water containing 1 mmol of $Y(NO_3)_3$ was added with vigorous stirring. Then, a 6 g solution in deionized water containing 4 mmol NH_4F was dropped in. The mixture was transferred to a 100 mL Teflon-lined autoclave and heated at 190 °C for 18 h.

Characterization. XRD patterns were recorded with a Bruker D8 diffractometer using Cu Ka radiation with 40 mA and 40 kV. Transmission electron microscopy (TEM) was carried out on a JEOL JEM-2010F electron microscope operated at 200 kV. Scanning transmission electron microscopy (STEM) was carried out using a JEOL JEM 2100F electron microscope operated at 200 kV, equipped with an Oxford INCA-IET200 detector for energy dispersion X-ray spectroscopy. XPS experiments were carried out on a Perkin-Elmer PHI-5000C ESCA system with Mg Kα radiation ($h\nu$ = 1253.6 eV) under a base pressure of 10^{-9} Torr. Decay curves were obtained using a Nd:YAG (EKSPLA PL2143A) laser coupled with an optical parameter oscillator (OPO) to give a wavelength tunable laser with pulse width of 30 ps. Emissions of 966 nm of Ho and 1058 nm of Nd were monitored with a digital oscilloscope synchronized to the single-pulse excitation. The photoluminescent lifetimes were obtained by fitting experiment data using a monoexponential decay equation for Ho and a biexponential decay equation for Nd in the OriginPro 8 software.

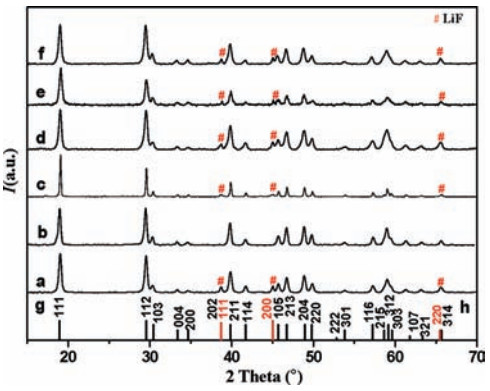

Figure 1. XRD patterns of $LiYF_4$ and $LiHoF_4$ nanocrystals synthesized under different conditions. (a) $LiYF_4$, 130 °C, 5 h, Li/Y/F = 23:1:4 (molar ratio). (b) $LiYF_4$, 130 °C, 5 h, Li/Y/F = 23:1.5:4. (c) $LiYF_4$, 130 °C, 5 h, Li/Y/F = 15:1.5:4. (d) $LiYF_4$, 160 °C, 5 h, Li/Y/F = 23:1:4. (e) $LiHoF_4$, 200 °C, 4 h, Li/Ho/F = 23:1:4. (f) $LiHoF_4$, 240 °C, 2.5 h, Li/Ho/F = 23:1:4. (g) LiF, JCPDS 45−1460 (red line). (h) $LiYF_4$, JCPDS 17−0874.

Results and Discussion

The XRD patterns in Figure 1 indicate that the obtained nanocrystals are of $LiYF_4$ and $LiHoF_4$, and all of the peaks can be indexed to the tetragonal phase of $LiYF_4$ (JCPDS 17−0874). When the molar ratio of Y/F is 1:4, there exists a small amount of LiF nanocrystals formed, but an excess of Y ions can completely eliminate the LiF phase at 130 °C for 5 h. However, in Figure 1c, when less LiOH is adopted, an excess of Y ions cannot completely eliminate LiF. Judging from the full-width at half-maximum (fwhm) of the XRD peaks in Figure 1a,b, the change in particle size of the nanocrystals induced by an excess of Y is not apparent. Transmission electron microscopy (TEM) and high-resolution TEM images of them are shown in Figure 2. Sphere-like $LiYF_4$ nanocrystals of about 50 nm can be obtained at 130 °C for 5 h, while octahedral-shaped nanocrystals with blunt edges and tips of about 150 nm are the products at 160 °C for 5 h. The SAED (selected area electron diffraction) pattern along the [−2 2 1] zone axis in the Figure 2a inset confirms that the $LiYF_4$ nanocrystal is a single crystal. From the SAED pattern along the [0 1 0] zone axis in the Figure 2b inset, we can determine that the octahedral nanocrystals are bounded by {1 1 2}, {−1 1 2}, {1 −1 2}, and {1 1 −2} facets. The regular shape of the $LiYF_4$ nanocrystal is particularly important for adjusting its orientation to an external magnetic field during magnetic measurements.[5] We can obtain $LiHoF_4$ nanocrystals at higher temperatures (Figure 1e,f). The $LiHoF_4$ nanocrystals obtained at 200 °C for 4 h and 240 °C for 2.5 h are both about 20 nm with an octahedral shape, shown in Figure 2d,e. The high-resolution (HR) TEM image in Figure 2e shows interplanar spacing of 0.303 nm corresponding to the (1 1 2) plane of the $LiHoF_4$ tetragonal structure. Energy-dispersive X-ray (EDX) analyses in Figure S1 (Supporting Information) of the products obtained using $Ho(NO_3)_3$ as a precursor reveals that the nanocrystals have a molar Ho/F ratio close to 1:4, demonstrating the formation of stoichiometric $LiHoF_4$.

(22) Wang, X.; Zhuang, J.; Peng, Q.; Li, Y. D. *Nature* **2005**, *437*, 121.
(23) Wang, L. Y.; Li, Y. D. *Nano Lett.* **2006**, *6*, 1645.
(24) Wang, X.; Zhuang, J.; Peng, Q.; Li, Y. D. *Inorg. Chem.* **2006**, *45*, 6661.

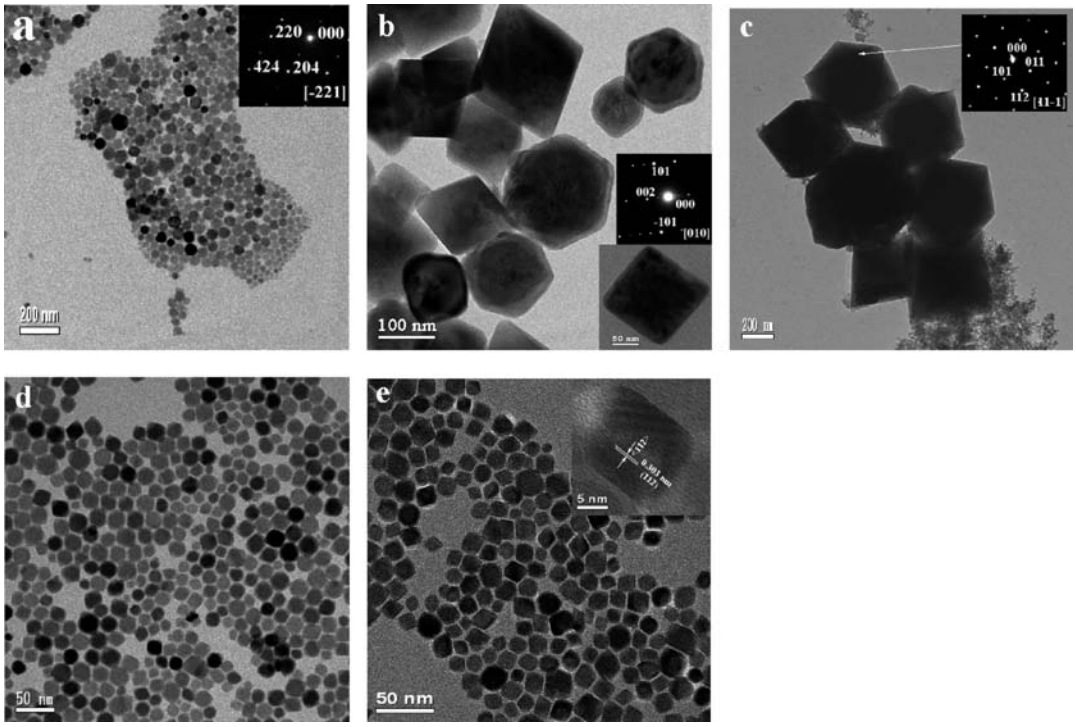

Figure 2. TEM images and SAED patterns of $LiYF_4$ and $LiHoF_4$ nanocrystals synthesized at different conditions listed in Figure 1. (a) Figure 1a, (b) Figure 1c, (c) Figure 1d, (d) Figure 1e, (e) TEM and HRTEM images of Figure 1f.

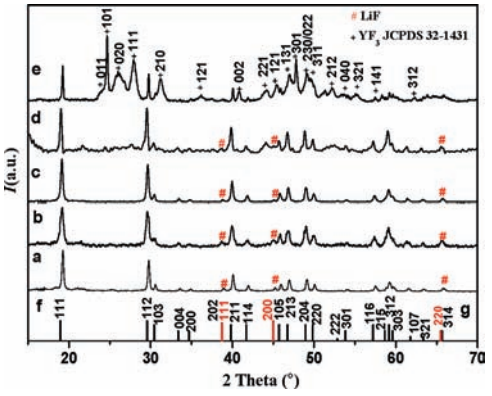

Figure 3. The XRD patterns of $LiYF_4$ nanocrystals synthesized under different conditions. (a) $LiYF_4$, 110 °C, 5 h Li/Y/F = 23:1.5:4 (molar ratio). (b) $LiYF_4$, 120 °C, 2.5 h, Li/Y/F = 23:1.4:4. (c) $LiYF_4$, 120 °C, 5 h, Li/Y/F = 23:1.25:4. (d) $LiYF_4$, 130 °C, 5 h, Li/Y/F = 7.6:1:4. (e) $LiYF_4$, 160 °C, 5 h, Li/Y/F = 6:1.25:4. (f) LiF, JCPDS 45−1460 (red line). (g) $LiYF_4$, JCPDS 17−0874.

By decreasing the concentration of LiOH with other parameters being identical, the XRD patterns indicate that the $LiYF_4$ nanocrystals can also be obtained. TEM images reveal that these $LiYF_4$ nanocrystals obtained by a lower concentration of LiOH possess an octahedral shape and a size of about 500 nm, with sharp edges and tips, shown in Figure 2c. However, when the amount of LiOH is less than a given value, mixed phases of $LiYF_4$ and YF_3 form in the case of Y, shown in the XRD pattern in Figure 3e. When the concentration of LiOH increases, the surface of the as-synthesized nanocrystals becomes irregular and rougher, and some of them possess a flower-like shape. The SAED pattern along the [1 1 −1] zone axis of one nanocrystal in the inset of Figure 4 indicates that it is still a single crystal. The concentration of LiOH determines the amount of oleates,

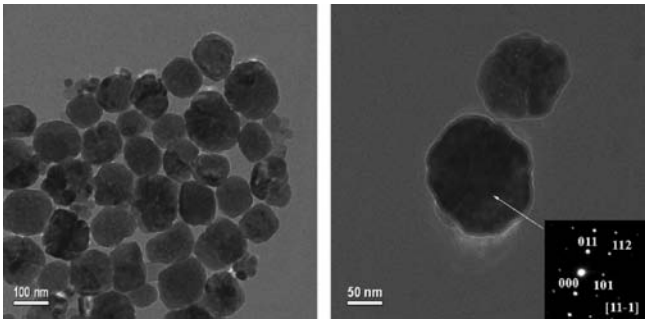

Figure 4. TEM images and SAED pattern of $LiYF_4$ nanocrystals synthesized with a higher concentration of LiOH at 160 °C for 5 h with a molar ratio of Li/Y/F = 31:1:4.

which are capping ligands during the growth of nanocrystals. The primary results indicate that the concentration of the capping ligands controls the growth kinetics of nanocrystals. We further investigate the process of crystallization under typical LiOH concentrations at lower temperatures. The XRD patterns in Figure 3a−c reveal that $LiYF_4$ and LiF phases form simultaneously at 110 and 120 °C. Comparing the TEM images and XRD patterns of $LiYF_4$ nanocrystals obtained under different conditions, we can come to a conclusion that the key factors in determining the size and shape of the nanocrystals and the phases of the products is the concentration of LiOH and the temperature.

For Ho, when the reaction temperature of 130 °C is selected and maintained for 5 h, the XRD patterns, in Figure 5a, indicate an unidentified phase and the LiF form. The XRD patterns in Figure 5b−e show that the pure $LiHoF_4$ phase can be obtained at 160 °C for 5 h or 180 °C for 2.5 h. However, a longer reaction time at 180 °C or higher, in Figure 1e,f, results in a mixed phase of $LiHoF_4$ and LiF. Unlike the formation of $LiYF_4$ and YF_3 at a very low LiOH concentration for Y,

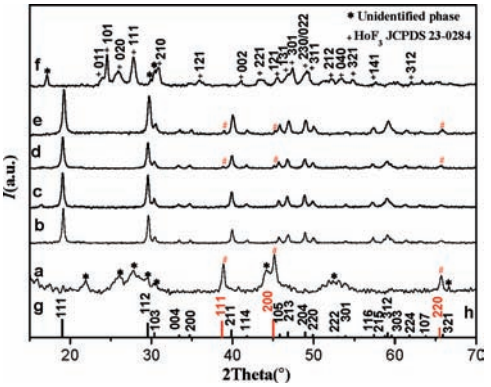

Figure 5. XRD patterns of $LiHoF_4$ nanocrystals synthesized under different conditions. (a) $LiHoF_4$, 130 °C, 5 h, Li/Ho/F = 23:1:4 (molar ratio). (b) $LiHoF_4$, 160 °C, 5 h, Li/Ho/F = 23:1:4. (c) $LiHoF_4$, 180 °C, 2.5 h, Li/Ho/F = 23:1:4 (d) $LiHoF_4$, 180 °C, 7.5 h, Li/Ho/F = 23:1:4. (e) $LiHoF_4$, 180 °C, 14 h, Li/Ho/F = 23:1:4. (f) $LiHoF_4$, 200 °C, 4 h, Li/Ho/F = 6:1:4. (g) LiF, JCPDS 45−1460 (red line). (h) $LiYF_4$, JCPDS 17−0874.

another unidentified phase and HoF_3 form (Figure 5f). In the case of Er, the XRD patterns in Figure S2 (Supporting Information) reveal that when the reaction temperature is at 110 °C for 5 h, only the LiF nanocrystal forms. When the temperature increases to 120 °C and is kept for 5 h, the $LiErF_4$ and LiF phases are obtained simultaneously. The large difference in the temperature and processes relative to the formation of neighbor $LiErF_4$ and $LiHoF_4$ nanocrystals is unexpected. For Tb and Dy, there are no nanocrystals obtained even at 200 °C for 4 h. The experimental phenomena of Y and Er−Lu are different from those of Ho, Dy, and Tb and can help to explain such differences in the temperature when obtaining nanocrystals. Before the addition of NH_4F solution, the solutions containing Y or Er−Lu are completely transparent, while there are precipitations for Ho, Dy, and Tb. This means the complexation of oleate and Y or Er−Lu is significantly different from that of Ho, Dy, and Tb. We tentatively assume that the complexes of Y or Er−Lu with oleate contain one Y or Er−Lu ion, and that the complexes of Ho, Dy, and Tb with oleate contain more than one, such as chain-like complexes. The dissociation and diffusion of the later complexes during the process of nucleation and growth are difficult, so a higher temperature for the formation of $LiHoF_4$, $LiDyF_4$, and $LiTbF_4$ nanocrystals is needed. In this regard, the ionic radii of RE ions, known as lanthanide contraction, correlates with the temperature of hydrothermal synthesis: the larger ionic radii, the higher the temperature. For REF_3, synthesized in published results,[24] rare earth ions (Y, Eu−Lu) all form REF_3 nanocrystals with an orthorhombic structure at the same temperature, 120 °C. The difference could arise from the incorporation of Li into the RE−F framework. This could give some clues to explain why the RE of hexagonal phase β-$NaREF_4$ nanocrystals is limited to Y and Er−Lu: a temperature of 230 °C is not enough for the formation of β-$NaHoF_4$ and other nanocrystals in that hydrothermal synthesis system.[25] The present hydrothermal synthesis approach is general and can produce other tetragonal-phase $LiREF_4$ nanocrystals, such as $LiTbF_4$, $LiDyF_4$, $LiTmF_4$, $LiYbF_4$, and $LiLuF_4$ (Figure S2 and S3, Supporting Information). TEM images of $LiTbF_4$ and $LiErF_4$ in Figure 6

(25) Zhang, F.; Wan, Y.; Yu, T.; Zhang, F. Q.; Shi, Y. F.; Xie, S. H.; Li, Y. G.; Xu, L.; Tu, B.; Zhao, D. Y. *Angew. Chem., Int. Ed.* **2007**, *46*, 7976.

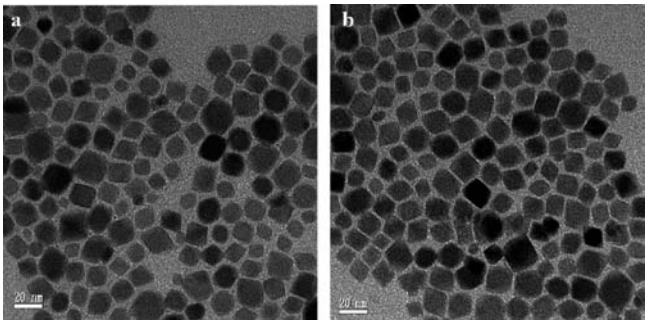

Figure 6. TEM images of $LiErF_4$ and $LiTbF_4$ nanocrystals synthesized under the conditions listed in Figures S2c and S3e (Supporting Information). (a) $LiErF_4$. (b) $LiTbF_4$.

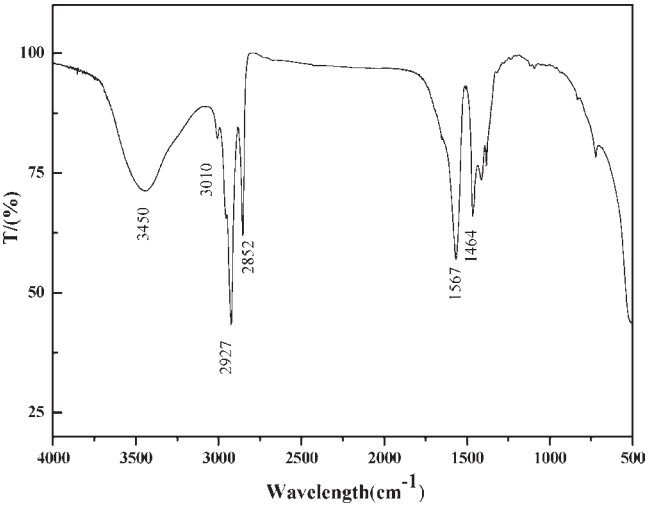

Figure 7. FTIR spectra of the $LiErF_4$ nanocrystal.

show that they are about 20 nm octahedra. Representative EDX spectra in Figure S4 (Supporting Information) indicate that $LiTbF_4$ and $LiErF_4$ nanocrystals have molar Tb/F and Er/F ratios close to 1:4. New rare earth fluorides are obtained in the cases of Gd and Eu, which will be published in a separate article. We also select low molecular weight multidentate acids instead of long-chain oleic acid to carry out hydrothermal synthesis in the absence of ethanol. Only a pure YF_3 phase can be generated by citric acid, and YF_3 and $LiYF_4$ mixed phases are obtained by iminodiacetic acid (Figure S5, Supporting Information). Without proper ligands, Li is not necessarily incorporated into the matrix of Y−F. These results indicate that the water−ethanol−oleic acid system is crucial in getting pure $LiYF_4$ phase.

The capping ligands on the surface of $LiErF_4$ nanocrystals are identified by FTIR spectra (Figure 7). The transmission bands at 2927 and 2853 cm^{-1} in both samples are respectively assigned to the asymmetric (ν_{as}) and symmetric (ν_s) stretching vibrations of methylene (CH_2) in the long alkyl chain. The peak at 3010 cm^{-1} attributed to the =C−H stretching vibration can clearly be seen in the spectrum. In addition, bands at 1567 and 1448 cm^{-1} are also found in the spectrum, associated with the asymmetric (ν_{as}) and symmetric (ν_s) stretching vibrations of the carboxylic group of the bound oleic acid. The sample exhibits a broad band at around 3450 cm^{-1}, probably corresponding to the O−H stretching vibration of the −COOH of absorbed oleic acid and water.[23] In addition, the existence of trace OH^- cannot be prohibited. But the

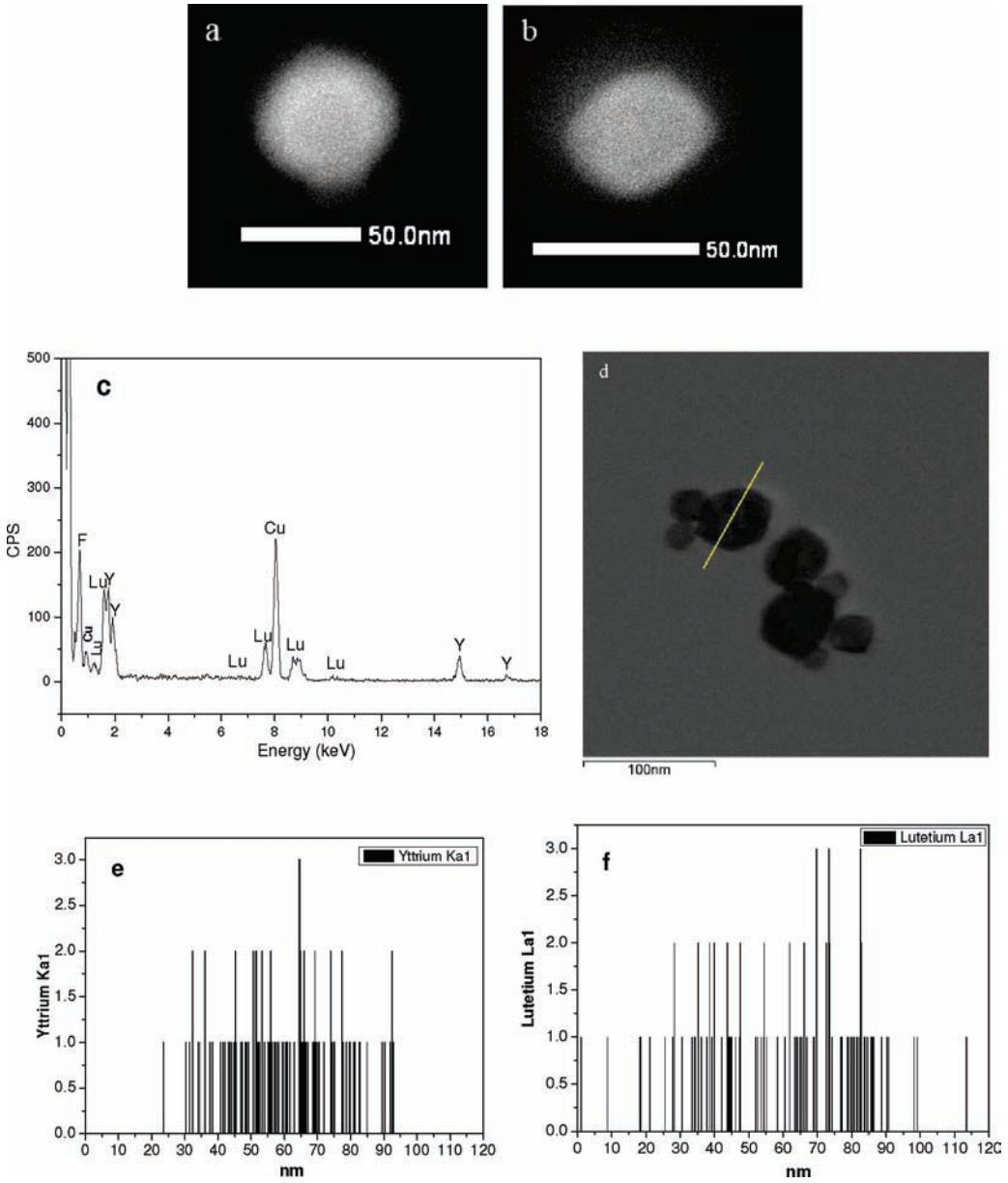

Figure 8. HAADF-STEM image and EDX-STEM of $LiYF_4-LiLuF_4$ core−shell nanocrystal. (a, b) HAADF-STEM images of two nanocrystals in dark field mode. (c) EDX analyses in STEM. (d) STEM image in bright field mode (yellow line is the region of the linear scan of Y and Lu). (e) EDX signals of Y (yttrium) along the selected line. (f) EDX signals of Lu (lutetium) along selected line. The Cu element is coming from the holey carbon film coated Cu grid supporting sample during STEM measurements.

OH^- can be largely eliminated as far as possible during the growth of nanocrystals by neutralization. So, in fact, it can be considered that there is very little OH^-, although it exists. The trace amount of oxygen in EDX spectra at 0.523 keV in Figures S1 and S4 (Supporting Information) and Figure 8c is appreciable for these molecules and oleate capping on the nanocrystal surface. Considering the excess amount of oleic acid compared with LiOH, the hydroxyl can largely be eliminated during the growth of nanocrystals.

We synthesized the $LiYF_4-LiLuF_4$ core−shell nanostructure according to the published method[18] and characterized it with scanning transmission electron microscopy in the high angle annular dark field mode (HAADF-STEM). The even brightness of the core and shell domains of the HAADF-STEM images in the dark field mode for sphere-like nanocrystals is consistent with light element Y in the core and heavy element Lu in the shell. EDX-STEM results of the single nanocrystal indicate that there are Y and Lu elements. A line profile across another core−shell nanocrystal shows that Y is only located in the core domain, while Lu presents throughout the whole nanocrystal and dominates in the shell (Figure 8d−f). The $LiHoF_4-LiErF_4-LiYF_4$ core−multishell nanostructure can also be obtained with this method. X-ray photoelectron spectroscopy (XPS) analysis in Figure S6 (Supporting Information) shows that the outer shell possesses the stronger XPS signal intensity of the corresponding rare-earth elements.

Ho- and Nd-doped $LiYF_4$ nanocrystals have been synthesized to investigate the photoluminescent properties. As shown in Figure 9, the PL lifetimes of $LiY_{0.955}Ho_{0.045}F_4$ and $LiY_{0.98}Nd_{0.02}F_4$ nanocrystals are obtained by measuring the relaxation of the $^5F_5$ excited state of Ho and the $^4F_{3/2}$ state

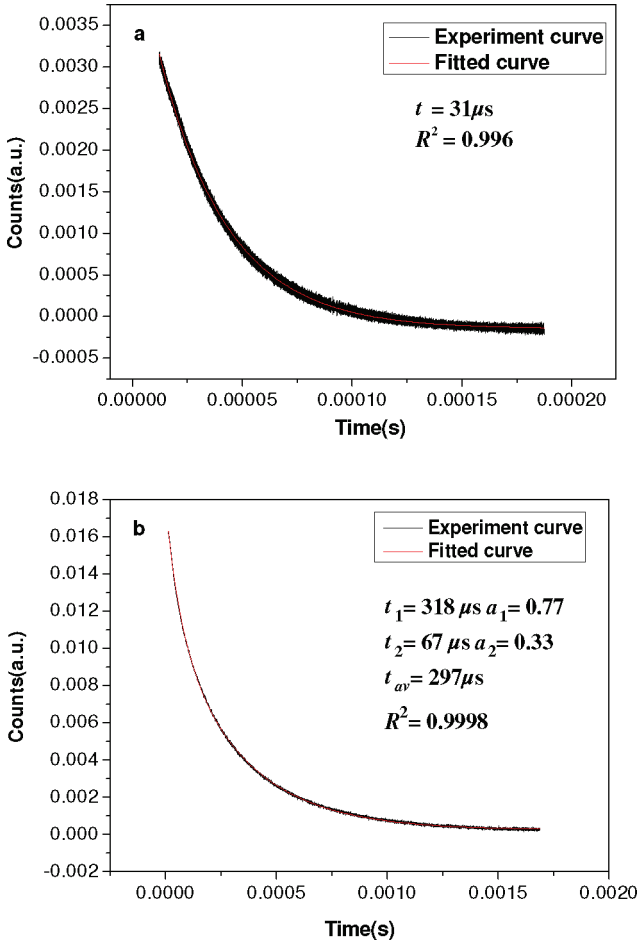

Figure 9. Decay curves for $LiY_{0.955}Ho_{0.045}F_4$ and $LiY_{0.98}Nd_{0.02}F_4$ nanocrystals. (a) $LiY_{0.955}Ho_{0.045}F_4$ nanocrystals excited at 545 nm and emission monitored at 966 nm at room temperature. (b) $LiY_{0.98}Nd_{0.02}F_4$ nanocrystals excited at 800 nm and emission monitored at 1058 nm at room temperature. $\tau_{av} = (\tau_1^2\alpha_1 + \tau_2^2\alpha_2)/(\tau_1\alpha_1 + \tau_2\alpha_2)$.[13] The units of τ_1, τ_2, and τ_{av} are microseconds, and α_i indicates the relative percentages of the different lifetime components.

of Nd and then fitting the experimental data with monoexponential and biexponential equations,[26] respectively. The PL lifetime of $LiY_{0.955}Ho_{0.045}F_4$ nanocrystals is 31 μs, very close to that of the $La_{0.95}Ho_{0.05}F_3$ nanocrystal.[27] The average PL lifetime of $LiY_{0.98}Nd_{0.02}F_4$ is 297 μs, comparable with the 390 μs of the $LiY_{0.985}Nd_{0.015}F_4$ fiber, with a lower Nd doping concentration.[4] The two lifetime components of the $LiY_{0.98}Nd_{0.02}F_4$ nanocrystal indicate that there are two kinds of Nd ion: inside the core and near the surface of $LiYF_4$ host. These results indicate that the distribution of the dopants in the $LiYF_4$ host nanocrystals obtained by solution-based hydrothermal synthesis is as uniform as that of the large single crystal synthesized using the Czochralski method.

Conclusions

In this article, we have revealed that the sizes and shapes of a series of $LiREF_4$ nanocrystals can be finely controlled by changing reaction conditions during the hydrothermal synthesis process, such as the LiOH concentration and temperature. The large difference in the temperature for the formation of different $LiREF_4$ nanocrystals is attributed to different precursors formed by oleate and rare earth ions. Complex core−shell nanostructures have been obtained and characterized by HAADF-STEM and XPS. Near-infrared emitting rare earth ion Nd- and Ho-doped $LiYF_4$ have been obtained, and photoluminescent properties have been investigated. These types of nanomaterials can be used as various kinds of rare earth phosphors in biolabels and nanocomposites and offer the opportunity to observe new or enhanced quantum behaviors on the nanoscale with the development of nanoSQUID and diamond-based ultrasensitive nanoscale magnetometry.

Acknowledgment. This work was supported by the National Natural Science Foundation of China (20971100) and Program for New Century Excellent Talents in University (NCET-08-0398).

Supporting Information Available: EDX of a $LiHoF_4$ nanocrystal. XRD patterns of $LiErF_4$ $LiTmF_4$, $LiYbF_4$, $LiLuF_4$, $LiDyF_4$, and $LiTbF_4$ nanocrystals. EDX spectra of $LiErF_4$ and $LiTbF_4$ nanocrystals. XRD patterns of the products synthesized with iminodiacetic acid or citric acid as stabilizing agents. XPS spectra of the $LiHoF_4$−$LiErF_4$−$LiYF_4$ core−shell nanostructure. This material is available free of charge via the Internet at http://pubs.acs.org.

(26) Stouwdam, J. W.; Hebbink, G. A.; Huskens, J.; van Veggel, F. C. J. M. *Chem. Mater*. **2003**, *15*, 4604.

(27) Stouwdam, J. W.; van Veggel, F. C. J. M. *Nano Lett*. **2002**, *2*, 733.